A mesoscopic model using the discrete element method for impacts on dry fabrics

Jérémie Girardot, Frédéric Dau

Matériaux & Techniques **104**, 408 (2016)

DOI: 10.1051/mattech/2016022
www.mattech-journal.org

Matériaux & Techniques

A mesoscopic model using the discrete element method for impacts on dry fabrics

J. Girardot[1,a] **and F. Dau**[1]

Received 14 March 2016, Accepted 22 June 2016

Abstract – Dry fabrics can be investigated in aeronautic field to contain debris. Such structures are most of the time modeled with finite elements leading to heavy time calculations especially due to contact treatment. An alternative way to compute efficiently contact treatment in case of textile under dynamic impact is proposed in this work. An original 3D Discrete Element Method (DEM) is carried out. It consists in a discrete representation of the fabrics at meso (yarn) and macro (textile) scales. The geometrical and mechanical modeling are first described taking into account a brittle elastic behavior for yarns and frictional contact between them. Then basic concepts of the DEM and the mesoscopic model with contact management are presented. An impact simulation scenario is performed to validate the implementation. Results are compared with simulations using the Finite Elements Method but also with available experimental datas.

Key words: Dry fabrics / fibers / impact / simulation / discrete element

1 Introduction

The weaving of high strength resistant yarns is commonly used in industrial applications as an impact energy absorber. Protective clothing, debris containment or textile-reinforced polymer are some examples of applications where dry fabrics made of stacking of 2D weaved plies (plain weaves or satin for instance) are largely encountered. Such dry fabrics are considered in this paper, involving impact velocity higher than 80 $m.s^{-1}$.

To simulate an impact on a dry fabrics and thus predict damages on the structure, two scales can be considered:

- the macromechanical approach consists in modeling the textile as a continuous media. A homogenized mechanical behaviour is adopted to simulate the fabrics deformation and failure using either the finite element method in [1, 2] or an analytical solving in [3, 4]. Discrete modeling approaches are also used in [5–7] by setting a mass-spring type network;
- at the mesomechanical scale, each yarns of the textile is explicitly modeled and the complex contact effects between the yarns during the impact is dealt with. The finite element method provides strain and stress fields in [8–11].

Other numerical approaches can be found in the literature but dedicated to different textile applications like the dry fabric forming using a mixed macro-mesoscale model in [12, 13] or the braiding and roving applications in [14, 15] where each fibers are modelled at the microscale.

For the ballistic impact, macro and meso approaches tend to predict the dry fabrics behavior and the projectile velocity. Comparison between these two scale approaches can be found in [10, 16]. It shows reasonable agreements between velocity measurements during an impact under fully fixed fabrics edges. Nevertheless, the friction between the yarns and the boundary conditions when two edges are fixed and the others free (for a rectangular fabrics) can not be properly described.

A mesomechanical approach is thus desirable to catch precisely local mechanisms mainly due to contact interaction between yarns. Using a standard finite element can lead to high CPU time when contacts are involved. While allowing a simple modeling of the yarns network including contacts, the present Discrete Element Methods [17] can be an efficient alternative to reduce time calculations. An original use of the DEM for continuous media is developed

[a] Corresponding author: jeremie.girardot@u-bordeaux.fr
[1] Institut of Mechanics and Mechanical engineering (I_2M), Dept. durability of materials, assemblies and structures Esplanade des Arts et Métiers, 33400 Talence, France

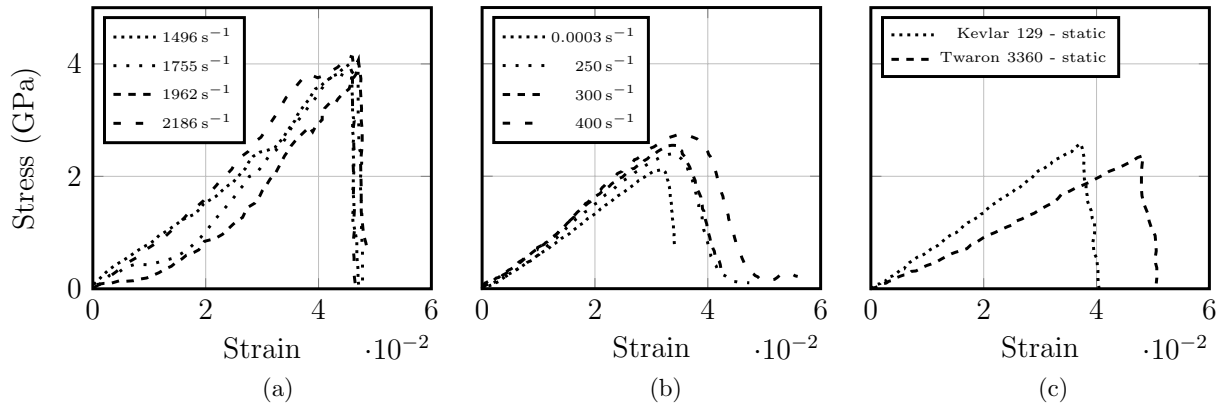

Fig. 1. Stress/strain curve for aramid [20] (a), Kevlar km2 [21] (b), and Kevlar 129 and Twaron 3360 [10] (c) at different strain rates.

in [18, 19], and is used in this work to model a yarn. The major benefits of this approach is the natural consideration of contacts between elements and a reduced time calculation using a temporal explicit integration scheme.

2 Mechanical model

2.1 Yarn behavior

The Figure 1 shows different results from the litterature with several stress/strain curves in longitudinal direction, for different kind of fiber material and at different strain rates. During these tests, several fibers are tested in the same time and thus the behavior is associated to the yarn one. It is relevant that a brittle linear elastic behavior is a good assumption to model a typical yarn material. In the present work, the yarn will be assumed to be a 2D-orthotropic material following a linear elastic behavior without strain rate dependencies. A brittle failure is assumed based on a maximum strain criterion. No damage laws are included in the model.

In agreement with the literature, several assumptions are done:

- transverse compression is neglected as its transverse modulus is small compared to the longitudinal modulus (more than a decade) [22];
- poisson effect, in-plane shear and bending stiffnesses are also neglected according to the parameter study performed in the same range of impact speed in [10]. In this work, it is also mentionned the value of the transverse stiffness has no influence on the macroscopic response of the textile during the impact. Therefore, a minimal value is required in order to well describe the itegrity of the yarn in the transverse direction.

These assumptions are reinforced by the fact that the impact velocity will remain up to 80 m.s^{-1} in our case. At this speed, no non-linear effect are observed yet like buckling or wrickling (effect especially coming from bending and compressive stiffnesses [23]).

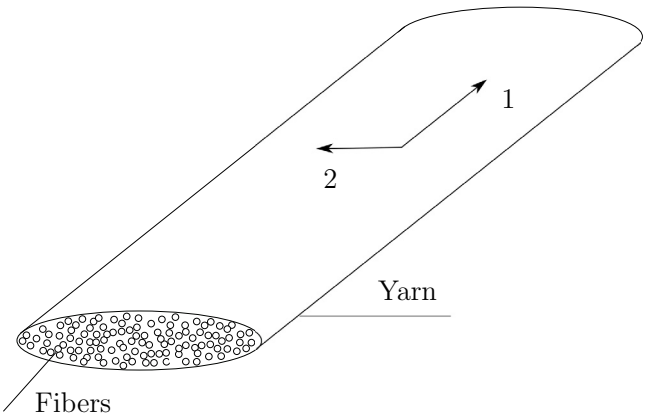

Fig. 2. Framework for yarn modeling.

The local frame is shown in Figure 2 with the 1-longitudinal direction and the 2-transverse one.

Strain-stress relation is then reduced to an in-plane behavior:

$$\begin{pmatrix}\varepsilon_{11}\\ \varepsilon_{22}\end{pmatrix} = \begin{pmatrix}\frac{1}{E_1} & 0\\ 0 & \frac{1}{E_2}\end{pmatrix}\begin{pmatrix}\sigma_{11}\\ \sigma_{22}\end{pmatrix}, \quad (1)$$

with E_1 and E_2, respectively denote the Young modulus in 1− and 2− direction. The yarn failure criterion is based on the maximum strain.

2.2 Contacts

Two contact interactions occur during an impact on a dry fabrics: the first between the yarns and the impactor and the second between the yarns themselves.

These contacts induce friction and in order to model it, a friction force $\overrightarrow{F_{\text{friction}}}$ is used. It is supposed to be proportional to the normal contact force $\overrightarrow{F_n}$ as:

$$\overrightarrow{F_{\text{friction}}} = \mu\left(||\overrightarrow{v_{\text{slip}}}||\right).||\overrightarrow{F_n}||.\frac{\overrightarrow{v_{\text{slip}}}}{||\overrightarrow{v_{\text{slip}}}||}. \quad (2)$$

The friction coefficient $\mu\left(||\overrightarrow{v_{\text{slip}}}||\right)$ is based on a regularized Coulomb law depending on the slipping velocity so

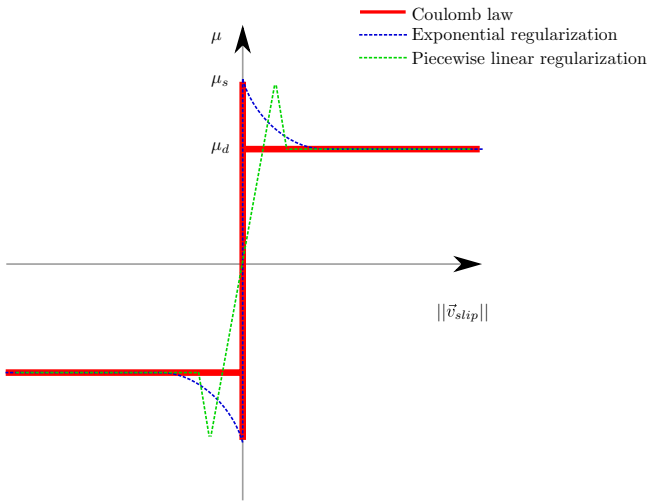

Fig. 3. Regularization laws for Coulomb contact model.

called $\overrightarrow{v_{\text{slip}}}$. This slipping velocity corresponds to the relative velocity between two bodies (for example between the impactor and on of the yarn of the fabric). Two friction coefficients are used to build the Coulomb law. The first coefficient corresponds to the static friction μ_s which is always greater than the second kinetic friction coefficient μ_k. The regularization function could be either a piecewise linear function or a decreasing exponential function below [11] (Fig. 3). Such an exponential regularization law is chosen and implemented in the present model (Eq. (3)).

The friction function $\mu\left(||\overrightarrow{v_{\text{slip}}}||\right)$ becomes:

$$\mu\left(||\overrightarrow{v_{\text{slip}}}||\right) = \mu_k + (\mu_s - \mu_k).\mathrm{e}^{-\alpha||\overrightarrow{v_{\text{slip}}}||}, \qquad (3)$$

where α is the exponential life time arbitrary fixed to 10^{-3}.

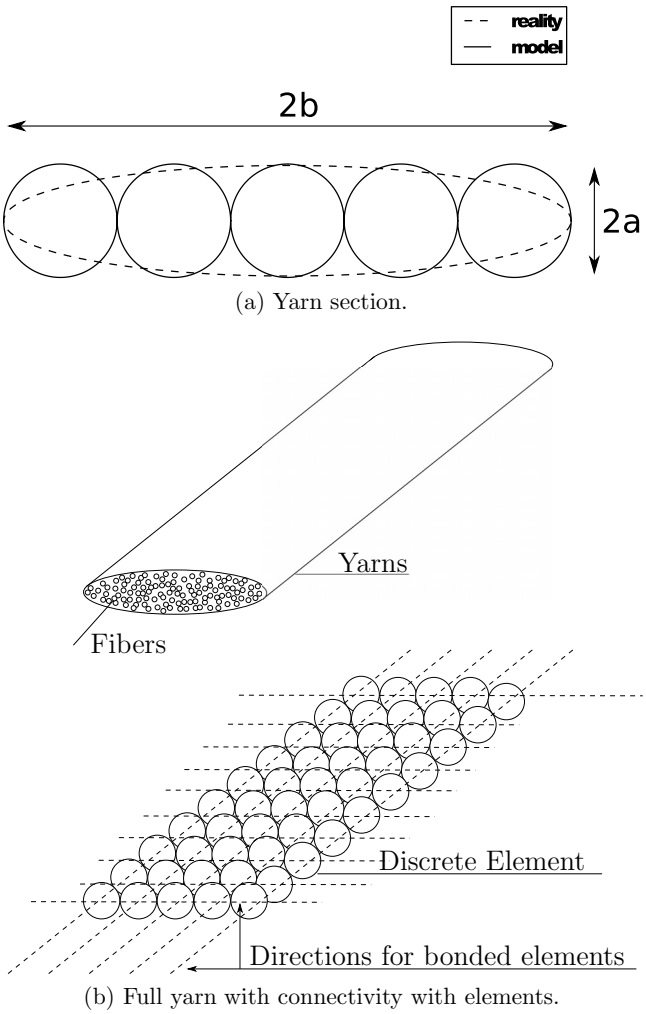

(a) Yarn section.

(b) Full yarn with connectivity with elements.

Fig. 4. Geometric yarn modelling.

3 DEM approach

3.1 Basic concepts

Originally, the DEM is suitable to model granular medias taking into account the contact between the grains. For instance, it has been useful to treat the friction between two bodies involving a third body [24]. The method has been recently extended [18] to model continuous media by using no-mass beams so that it could be used to deal with the continuous phase of the media before it becomes discontinuous when cracks occur. The present DEM is then able to manage cracks propagations inside the media with no extra numerical difficulties. Moreover, its ability to easily catch contacts between several parts tends to make the DEM be a relevant method to simulate impacts on dry fabrics.

Inertia of the considered media is concentrated on the Discrete Elements (DE). The DE shape depends on the nature of the physical problem adressed. In the present study, a spherical shape is adopted.

The numerical solving consists in satisfying the dynamical equilibrium of each element subjected to external forces (contact and mechanical behavior) using an explicit integration scheme [19].

The next section deals with the geometric modelisation of the yarn with spherical DEs.

3.2 Geometric modelisation

Each yarn is modeled as a deformable body following the mechanical behavior presented in Section 2.1. It is discretized using multiple discrete elements, as it could be done with FE [11]. DE are uniformly distributed in the yarn section, supposed to be elliptical (Fig. 4a). At this stage, improving the description of the elliptic section by adding DE is out of the scope. These elements are connected each other following a grid pattern which represents the orthotropic behavior (see Fig. 4b). Same diameter and density are adopted for each DE. The DE are kept spherical to prevent from heavy calculations due to the contact treatment. As the representation of a yarn with spaced spherical shapes is not naturally, a sensitivity

analysis on the discretization thiness of the grid pattern is presented in the beginning of Section 4.2.3. Several geometric configurations with different DE overlappings (up to 70%) have been tested. No significant influence on the results (impact velocity and rupture mechanisms) has been observed. So, the yarn modelisation shown in Figure 4a is a good compromise for impact simulations.

The fabrics result is shown in Figure 5a with its associated connectivity pattern (Fig. 5b). The weaving is a 2D plain and the trajectories of yarns are built with periodic sinusoisidal functions such that no interprenetrations occur between all the DEs, and also to respect the crimp coefficient of the fabric.

3.3 Mechanical behavior in the DEM

3.3.1 Yarn inertia

The DE density is simply determined by writting the mass equality between the real yarn and its geometric representation. It leads to the following expression of the density ρ_{micro} of each DE:

$$\rho_{\text{micro}} = \rho_{\text{macro}} \frac{3abL_{\text{yarn}}}{4N_{yarn}R^3}, \tag{4}$$

with R, L_{yarn}, ρ_{macro} and N_{yarn} respectively denote the DE radius, the length of the yarn, the yarn density and the number of DEs in the yarn section. a and b are the semi-minor and semi-major axis of the ellipse, drawn in Figure 4a.

3.3.2 Yarn stiffness

Mechanical behavior in the DEM is modeled thanks to bonds connected between DE described in the previous section. The 2D-orthotropic behavior of yarns is modeled with a pattern of longitudinal and transversal no-mass springs. Each spring is connected to two adjacent discrete elements. Two different stiffnesses are considered: K_1 for the longitudinal springs (direction 1) and K_2 for the transversal ones (direction 2). K_2 is assumed to be proportional to K_1. The ratio $\frac{K_1}{K_2} = 10$ will be adopted after sensitivity analysis (see Sect. 4.2). It will be observed that the main role of this transverse stiffness is to ensure the yarn cohesion in the transverse direction during the impact.

K_1 can be easily obtained from material and geometrical parameters:

$$K_1 = \frac{E_1 S}{N_2 2R}, \tag{5}$$

$$K_2 = 10K_1, \tag{6}$$

where E_1, R, S, and N_2 are respectively the Young modulus in 1−direction, the radius of a spherical DE, the area of the yarn section and the number of DE in the transverse direction.

Finally, each spring exerts two forces $\overrightarrow{F_{s/1}}$ and $\overrightarrow{F_{s/2}}$ respectively on the two discrete elements at its ends (noted 1 and 2) expressed as:

$$\text{(a)} \begin{cases} \overrightarrow{F_{s/1}} = \quad K_i \Delta L \overrightarrow{n}, \\ \overrightarrow{F_{s/2}} = -K_i \Delta L \overrightarrow{n}, \end{cases} \text{(b)} \ \frac{\Delta L}{L_0} = \varepsilon_{\max}, \tag{7}$$

where $K_i (i \in [1,2])$ is the corresponding longitudinal or transversal stiffness, ΔL the difference between the current length and the initial length L_0 of the spring and $\overrightarrow{n}$ the normalized vector of the support joining the centers of two adjacent DE. When the failure criterion is reached, (Eq. (7)b), the spring is removed from the calculation.

3.3.3 Contact management

The contact between DE is naturally taken into account. When an interpenetration is detected (i.e. when the distance between two DE centers becomes smaller than the sum of the DE radii), the reaction force $\overrightarrow{F_n}$ which takes place betwen the DEs is computed as:

$$\overrightarrow{F_n} = \pm \delta K_c \overrightarrow{n}, \tag{8}$$

where δ represents the interpenetration between two DEs and $\overrightarrow{n}$ the unit normalized support vector. The contact stiffness K_c is assumed to be the same order of magnitude as K_1 by numerical convenience and after sensitivity analysis.

The friction is taken into account by applying a tangential force $\overrightarrow{F_t}$ using the friction coefficient μ and the previously computed normal contact force:

$$\overrightarrow{F_t} = \mu\left(||\overrightarrow{v_{rel}}||\right) ||\overrightarrow{F_n}|| \frac{\overrightarrow{v_{rel}}}{||\overrightarrow{v_{rel}}||}, \tag{9}$$

where $\overrightarrow{v_{rel}}$ is the relative velocity in the tangential plane between two DE. It is obtained by a projection of the velocity difference in the tangential plane:

$$\overrightarrow{v_{rel}} = (\overrightarrow{v_1} - \overrightarrow{v_2}) - \overrightarrow{n}.(\overrightarrow{v_1} - \overrightarrow{v_2}).\overrightarrow{n}. \tag{10}$$

The function $\mu\left(||\overrightarrow{v_{rel}}||\right)$ comes directly from the Equation (3).

4 Impact simulation on plain weave textile

4.1 Sensitivity analysis

Several simulations of impact are performed on a 154 mm×154 mm square plain weave ply fully clamped on its edges. The diameter projectile is 4 mm diameter, and its initial velocity is 40 m.s^{-1}. The geometry parameters for the yarns and the textile are detailed in Table 1:

– the width and the thickness of each yarn (related to the parameters a and b in Fig. 4a) ;

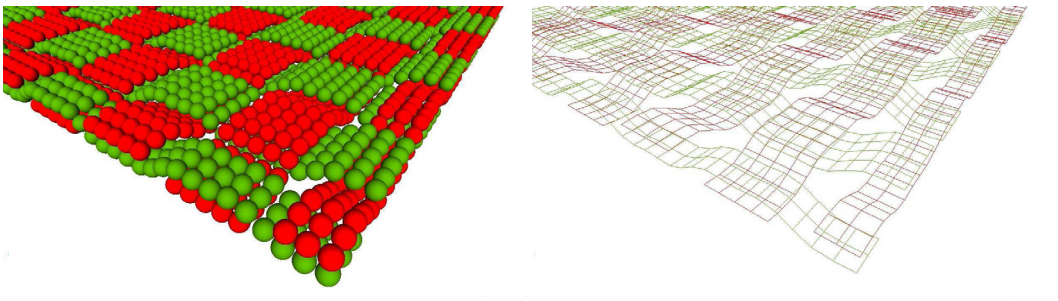

(a) (b)

Fig. 5. Final Fabrics representation with the warp yarns in green and the weft yarns in red (a), and its associated connectivity (b).

Table 1. Input parameters for the sensitivity analysis.

Yarn width	(mm)	0.59
Yarn thickness	(mm)	0.115
–		
Distance between yarns	(mm)	0.746
Thickness	(mm)	0.265
Crimp	(%)	4.12
–		
Longitudinal stiffness	$M.N.m^{-1}$	5
Transversal stiffness	$M.N.m^{-1}$	5
Contact stiffness	$M.N.m^{-1}$	5
Density	$kg.m^{-3}$	1000
Failure strain	%	5
Static friction μ_s		0.2
Dynamic friction μ_d		0.2

– the distance between two yarns (adequate parameter for a plain weave), the final thickness and the crimp of the weaving.

The longitudinal and transverse stiffnesses, the contact stiffness, the density and the failure strain are the chosen parameters to perform the sensitive analysis. The basic configuration for this sensitivity analysis (basic value for the parameters) is also included in Table 1. Static and dynamic friction coefficients are both equal to 0.2.

The effects of those parameters is appreciated on the response of the projectile velocity versus the time. The Figure 6 shows the typical displacement field during the begining of the impact, meaning before any yarn failure. For a better understanding, the spherical impactor is not plotted. The displacement is null around each boundaries of the fabrics the deformation of the textile is maximal under the projectile and spreads along the yarns.

In Figure 7, each projectile velocity curve is plotted.

Figure 7a shows the results from simulations using different values of longitudinal, transverse and contact stiffnesses. The values of these parameters are 2 $M.N.m^{-1}$, 5 $M.N.m^{-1}$ and 8 $M.N.m^{-1}$. It appears that only the longitudinal stiffness modifies the macroscopic response of the projectile velocity. As expected, the more the yarn is rigid, the more it slows down the projectile. It is observed that contact stiffnesse has no influence on the projectile velocity.

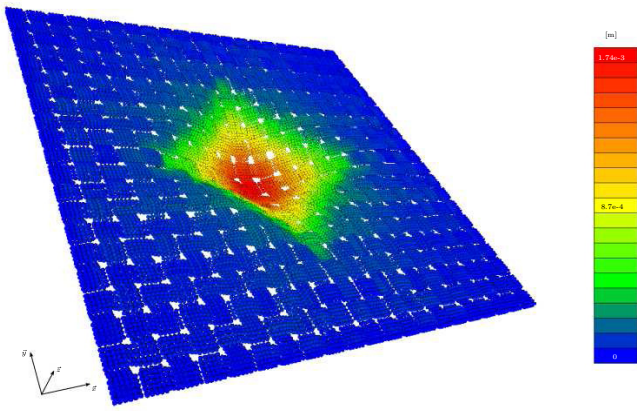

Fig. 6. Out-of-plane displacement field (z) [m] at the beginning of an impact ($v_{\text{projectile}} = 40$ $m.s^{-1}$).

In Figure 7, each curve corresponds to simulation using a different failure strain. The black dots represent the first failure in the textile which always occurs in the location under the projectile. The failure strain has no influence on the first part of the velocity curve but does have on the moment of the first failure. After the first failure, the projectile is passing through the textile and a residual velocities of 17.2 m/s and 23.8 m/s are obtained respectively for failure strains equal to 4% and 3%. For a strain failure of 5%, a failure is observed but is not sufficient for the total break down of the textile. For a strain failure of 6%, no failure occurs.

In Figure 7, it appears that the yarn density has an influence only on the beginning of the impact where the uncrimping mechanism is occuring. However, it does not play a major role on the projectile velocity. Indeed, with a range of value of density from 500 to 3000 $kg.m^{-3}$, the projectile always reach a velocity of 20 $m.s^{-1}$ at the time 75 μs.

For all simulations, the results plotted in Figure 7 show a very good numerical stability using the Verlet explicit time integration scheme without any artificial damping added. Our implementation is self-stable.

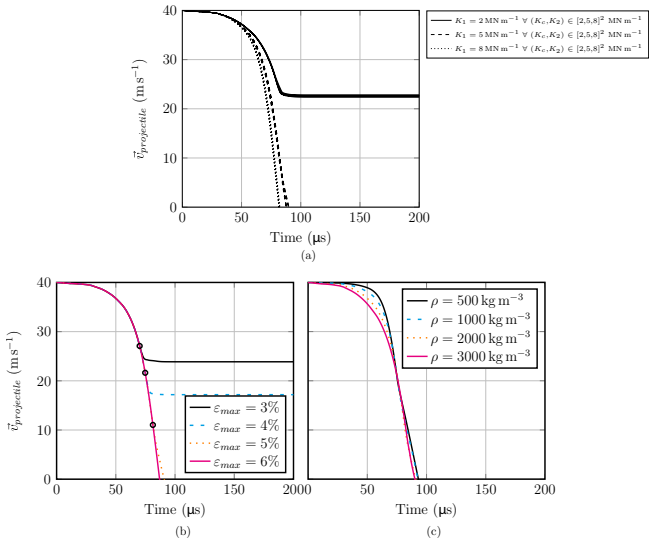

Fig. 7. Projectile velocity during the impact for various input parameters: (a) longitudinal, transversal and contact stiffnesses, (b) failure strain (black circles point out the first failure) and (c) density.

Table 2. Input parameters based on [10].

Yarn Modulus E_1	(GPa)	62
Yarn width	(mm)	0.59
Yarn thickness	(mm)	0.115
Yarn density	($\mathrm{kg.m^{-3}}$)	1310
Yarn failure strain	%	5.48
–		
Distance between yarns	(mm)	0.746
Thickness	(mm)	0.265
Crimp	(%)	4.12
–		
yarn/yarn static friction		0.23
yarn/yarn dynamic friction		0.19
impactor/yarn static friction		0.18
impactor/yarn dynamic friction		0.18

4.2 Real impact test

A 5 cm×5 cm square plain weave ply of Kevlar fibers with two clamped edges and two free edges is considered in this experimentation based on [10]. Three projectile velocities are addressed: 60 $\mathrm{m.s^{-1}}$, 90 $\mathrm{m.s^{-1}}$ and 245 $\mathrm{m.s^{-1}}$. Only a quarter of the domain is modeled thanks to the double symmetry of the plain weaving. The projectile is a rigid sphere with a diameter of 5.35 mm. The impact is located at the center of the fabrics, at the cross intersection of two yarns. Datas needed for simulations are summarized up in Table 2.

4.2.1 Qualitative results

Figure 8 shows the damage progression during impact. A well-known pyramidal shape deformation is retrieved (Fig. 9). The unweaving caused by the impact as well as the yarns failure under the projectile can be captured.

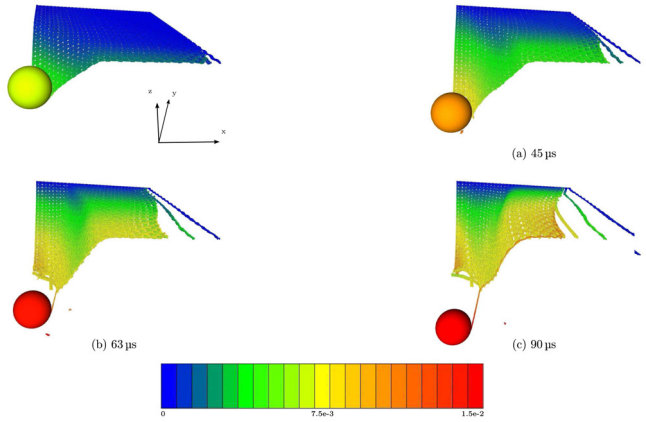

Fig. 8. Out-of-plane displacement field (z) [m] at different times for the impact at 245 $\mathrm{m.s^{-1}}$.

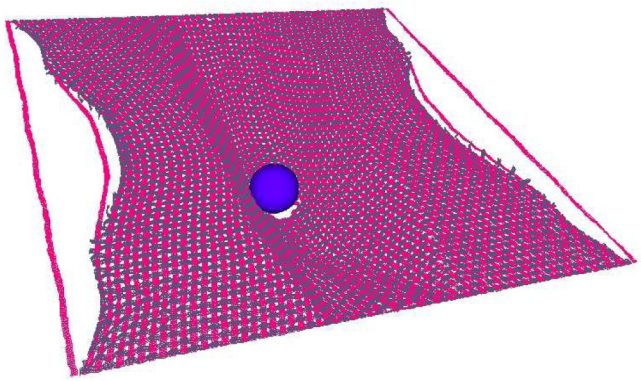

Fig. 9. Typical pyramidal shape during an impact.

The opposition of a yarn, initially not fixed at its ends, accompanying the projectile until it passes through the textile is remarkable, Figure 8c.

CPU time for this calculation is between 7 h for the 60 $\mathrm{m.s^{-1}}$ velocity impact and 2.5 h for the 245 $\mathrm{m.s^{-1}}$ one. These times are greatly lower than these observed in similar simulations using FEM [10] where CPU time are around 17 hours and 8 hours for the same impact velocities.

4.2.2 Energy balance

This study was the opportunity to compute the energy balance during an impact. Thus, strain energy, contact energies (due to stiffness and friction) and kinetic energies (for the fabrics and for the projectile) can be assessed at each time of calculation. The energy balance during the impact at 245 $\mathrm{m.s^{-1}}$ is plotted in Figure 10a. The projectile kinetic energy decreases until the last yarn failure occurs (at time around 80 μs), then it remains constant. On the same time, a competition occurs between woven kinetic and strain energies. When a failure occurs in the fabric, the stored strain energy is released and transferred into kinetic energy. Friction effects during the impact induce a constant increasing energy. One can verify that the

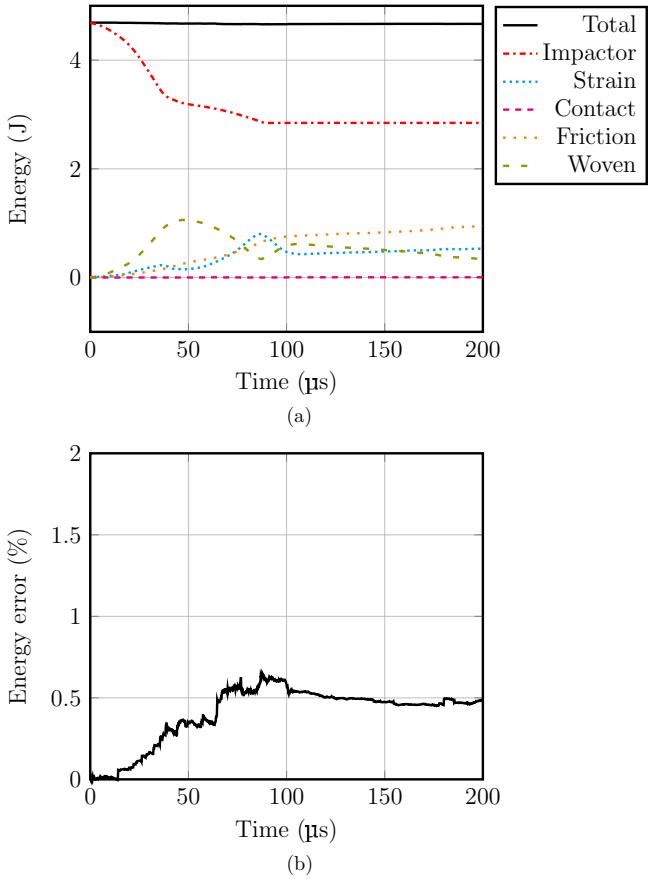

Fig. 10. Energy balance (a) and energy conservation error (b) during an impact at 245 m.s^{-1}.

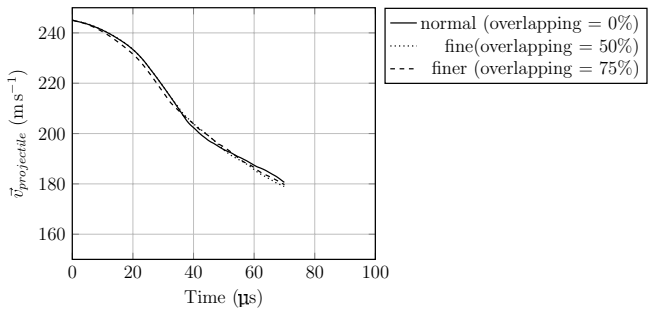

Fig. 11. Projectile velocity with an initial velocity of 245 m.s^{-1} for an increasing overlapping of the Discrete Elements in the grid pattern geometry.

energy due to the artificial contact stiffness (named contact in Fig. 10a) is insignificant compared to the others.

Finally, the conservation energy error during the simulation can be evaluated (Fig. 10b). During the simulation, it never exceeds 0.7%.

4.2.3 Projectile velocity

First of all, a discretization analysis is performed and the impactor velocity is plotted in Figure 11 for three different thinesses for the grid pattern: *normal*, *fine* and *finer*. They correspond respectively to an (overlapping = 0%), fine (overlapping = 50%), finer (overlapping = 75%). Despite a better representation of the surface due to the overlapping, the impactor velocity evolution remains the same, whatever the discretization is. Consequently, in order to keep good numerical performance, the *normal* grid pattern is always used. The reader should notice that only a high velocity impact is performed for this analysis.

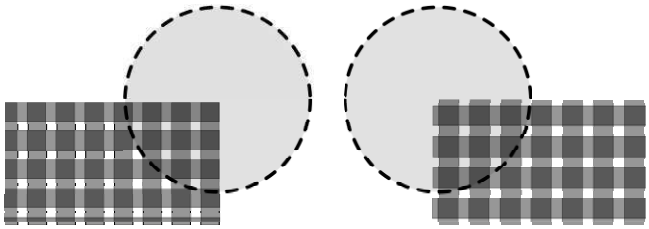

Fig. 12. Two different impact locations: at the cross intersection of two yarns (left) and between four yarns (right).

The evolution of the projectile velocity is plotted in Figure 13a for the three initial impactor velocities: 60 m.s^{-1}, 90 m.s^{-1} and 245 m.s^{-1}. DEM results are compared with FEM results [10]. For each velocity, DEM and FEM results are coincident at the beginning of impact; the "decrimping" of the fabrics is well described. In contrast, they don't match when the first yarn failures occur resulting in a change of slope. This change appears later with DEM. Nevertheless, the slope becomes zero when the projectile passes through the fabrics; its velocity remains constant. A second change of slope is observed for the 245 m.s^{-1} impact which is not observed for the FEM results. It is due to friction between the impactor and the fabrics after the yarn failures. This phenomenon is also observed in more recent simulation work using FEM in [25]. Results for 60 and 90 m.s^{-1} are qualitatively in a good agreement with those found in [10].

DEM results are also compared with an experimental measurement found [26] for the initial impact velocity of 245 m.s^{-1}, presented in Figure 13b. Two impact locations are also considered: the first is located at the cross intersection of two yarns (noted *cross* in Fig. 13b) and the second is located on the space between four cross intersection (noted *space* in Fig. 13b). The Figure 12 illustrates these two conditions. The predicted residual impactor velocity for the *cross* condition is 185 m.s^{-1} whereas experimental result [26] and FEM prediction [10] respectively give 207 m.s^{-1} and 5m.s^{-1}. So, it is underestimated with DEM and overestimated with FEM. However, the *space* condition leads to a good agreement with the experimental value of 207 m.s^{-1}. Indeed, this condition seems to represent better the reality of an impactor in contact with a fabrics.

5 Conclusion

Present results clearly show the capabilities of the DEM to deal with impact on dry fabrics at mesoscopic scales. Qualitative results are mainly demonstrated in this

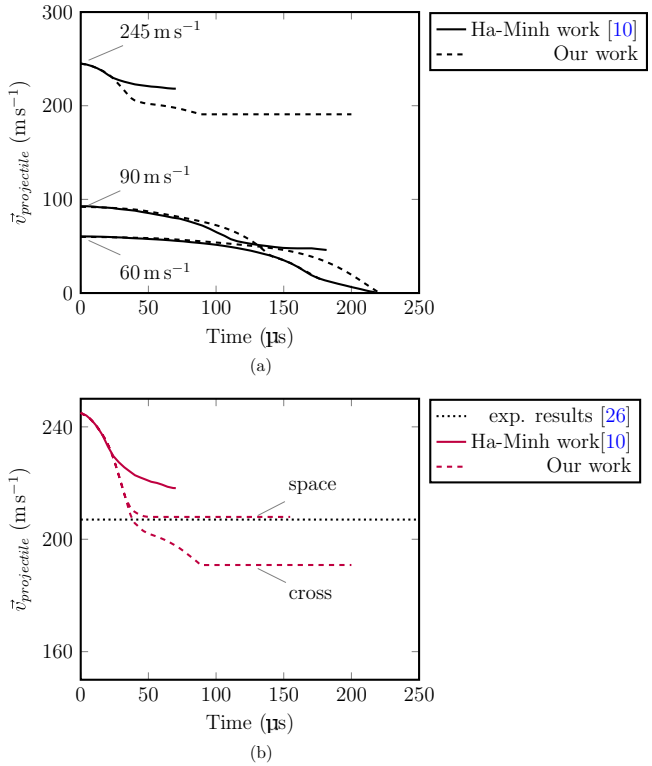

Fig. 13. Predictions and measurements of projectile velocity for various impact velocity .

paper but quantitative results are encouraging. It also shows the advantage of a mesoscopic approach to simulate impact on fabrics and correctly predict the residual velocity.

But one of the major advantage using the DEM is the time calculation which is at least three times smaller than a simulation using the FEM. Simplicity of the mechanical model using bonds between discrete elements and the dedicated LCM (Link Cell Method) contact detection algorithm [17] are the main reasons.

Future impacts simulations will be performed on the interlock 3X weaving varying the number of DE and impact conditions to analyze the mass and velocity impactor but also the prestressed effects on global responses and failure progression in the textile. Then, coupling DE model to a continuous one is intended to be able to model larger woven target. Dry fabrics in hybrid structures (CFRP + Textile) for impact applications are also explored. Draping fabrics is another possible use of the method, not yet investigated.

Acknowledgements. All the development in this work were done thanks to the GranOO workbench (http://www.granoo.org/).

This work is supported by the National Research Agency (ANR) trough the VulComp2 project (#ANR-12-RMNP-0018-07).

References

[1] A. Shahkarami, R. Vaziri, *Int. J. Impact Eng.* **34** (2007) 104-119
[2] C. Lim, V. Shim, Y. Ng, *Int. J. Impact Eng.* **28** (2003) 13-31
[3] H. Billon, D. Robinson, *Int. J. Impact Eng.* **25** (2001) 411-422
[4] C. Ha-Minh, A. Imad, F. Boussu, T. Kanit, *Compos. Struct.* **99** (2013) 462-476
[5] B. Ben Boubaker, B. Haussy, J.F. Ganghoffer, *Comptes Rendus Mécanique* **335** 007) 150-158
[6] K. Joo, T. Jin Kang, *Textile Res. J.* **77** (2007) 359-368
[7] D. Jauffrès, J.a. Sherwood, C.D. Morris, J. Chen, *Int. J. Mater. Forming* **3** (2009) 1205-1216
[8] Y. Duan, M. Keefe, T. Bogetti, B. Cheeseman, *Compos. Struct.* **68** (2005) 331-337
[9] Y. Duan, M. Keefe, T. Bogetti, B. Powers, *Int. J. Mecha. Sci.* **48** (2006) 33–43
[10] C. Ha-Minh, A. Imad, T. Kanit, F. Boussu, *Int. J. Mech. Sci.* **69** (2013) 32-39
[11] M. Rao, Y. Duan, M. Keefe, B. Powers, T. Bogetti, *Compos. Struct.* **89** (2009) 556-566
[12] P. Boisse, K. Buet, A. Gasser, J. Launay, *Compos. Sci. Technol.* **61** (2001) 395-401
[13] P. Boisse, A. Gasser, B. Hagege, J.L. Billoet, *J. Mater. Sci.* **40** (2005) 5955-5962
[14] D. Durville, *Int. J. Mater. Forming* **3** (2010) 1241-1251
[15] T. Vu, D. Durville, P. Davies, *Int. J. Solids Struct.* **58** (2015) 106-116
[16] M. Grujicic, W.C. Bell, G. Arakere, T. He, X. Xie, B.a. Cheeseman, *J. Mater. Eng. Perform.* **19** (2009) 22-39
[17] D. André, J.l. Charles, I. Iordanoff, J. Néauport, *Adv. Eng. Software* **74** (2014) 40-48
[18] D. André, I. Iordanoff, J.l. Charles, J. Néauport, *Comput. Methods Appl. Mech. Eng.* **213-216** (2012) 113-125
[19] D. André, M. Jebahi, I. Iordanoff, J.l. Charles, J. Néauport, *Comput. Methods Appl. Mech. Eng.* **265** (2013) 136-147
[20] V. Tan, X. Zeng, V. Shim, *Int. J. Impact Eng.* **35** (2008) 1303-1313
[21] M. Cheng, W. Cheng, T. Weerasooriya, *J. Eng. Mater. Technol.* **127** (2005) 197-203
[22] Y. Duan, M. Keefe, T. Bogetti, B.a. Cheeseman, B. Powers, *Int. J. Impact Eng.* **32** (2006) 1299-1312
[23] P. Boisse, N. Hamila, E. Vidal-Sallé, F. Dumont, *Compos. Sci. Technol.* **71** (2011) 683-692
[24] I. Iordanoff, B. Seve, Y. Berthier, *J. Tribol.* **124** (2002) 530
[25] Y. Wang, X. Chen, R. Young, I. Kinloch, *Compos. Struct.* **135** (2016) 8-16
[26] M. Alves, N. Jones, Impact loading of lightweight structures, (Southampton; Boston, Mass.: WIT Press), 2002